

## STATISTICAL CORRECTION OF CENTRAL SOUTHWEST ASIA WINTER PRECIPITATION SIMULATIONS\*

MICHAEL K. TIPPETT<sup>†</sup>, MATHEW BARLOW and BRADFELD LYON

*International Research Institute for Climate Prediction, Columbia University, Palisades, NY, USA*

June 18, 2003

### ABSTRACT

Severe drought is a notable feature of the hydrology of Central Southwest (CSW) Asia. Although studies have linked the region's interannual precipitation variability to remote forcings that include East Asia Jet Stream variability and Western Pacific tropical convection, atmospheric general circulation models (GCMs) forced by observed sea surface temperatures demonstrate little skill in simulating interannual precipitation variability in this region. Here statistical methods of correcting systematic errors in GCM simulations of CSW Asia precipitation are investigated. Canonical correlation analysis is used to identify model fields related to observed precipitation anomaly patterns. These relationships are then used to predict observed precipitation anomalies. This approach is applied to the ECHAM 4.5 GCM using regional precipitation, upper-level winds and Western Pacific tropical precipitation as predictors of observed CSW Asia precipitation anomalies. The statistical corrections improve the GCM precipitation simulations, resulting in modest, but statistically significant, cross-validated skill in simulating CSW Asia precipitation anomalies. Applying the procedure to hindcasts with persisted sea surface temperatures gives lower, but statistically significant, precipitation correlations in the region along the Hindu Kush mountain range.

KEY WORDS: Central Southwest Asia precipitation, Afghanistan, East Asia Jet Stream, CCA.

### 1. INTRODUCTION

Much of Central Southwest (CSW) Asia has a semi-arid climate with precipitation primarily resulting from eastward-propagating mid-latitude cyclones during the cold season (Martyn, 1992). A substantial fraction of the region's annual precipitation falls along the slopes of the region's principal mountain ranges during winter and early spring, mostly in the form of snow. The melting of this snow provides an important source

\* International Research Institute for Climate Prediction Contribution Number IRI-PP/03/01.

<sup>†</sup> Corresponding author. IRI, 223 Monell, Lamont Campus, 61 Route 9W, Palisades New York 10964-8000. Phone: 845-680-4420 Fax: 845-680-4865 email: tippett@iri.columbia.edu

of water during the summer. Regionally much of the winter precipitation occurs, on average, in Northeast Afghanistan and Tajikistan and on the Southwest border of Iran. Interannual precipitation variability is large and includes episodes of severe drought, with CSW Asia recently experiencing four years (1998-2002) of the worst drought in fifty years (Barlow *et al.*, 2002). Societal impacts of the drought were severe, with agricultural production and livestock populations, both key to subsistence livelihoods in the region, being drastically reduced (Agrawala *et al.*, 2001).

Seasonal forecasts of CSW Asia precipitation anomalies would be feasible if CSW Asia precipitation were related to predictable components of the climate system such as ENSO. However, the CSW Asia region is not typically noted as part of the ENSO signal (Ropelewski and Halpert, 1987, 1989), although Nazemosadat and Cordery (2000) have recently documented an ENSO signal in Iran using a higher density of stations than previously examined. In addition to data availability is the issue of the variation of sea surface temperature (SST) anomaly patterns from one ENSO event to another. Some ENSO events appear to have more impact on CSW Asia precipitation than others. Barlow *et al.* (2002) stratified ENSO events based on the strength of their Western Pacific SST anomalies and found precipitation and circulation anomalies in the Western Pacific, Eastern Indian Ocean, and extending into Asia that were different from usual ENSO-related patterns. The ENSO stratification with the more vigorous Western Pacific SST signal is associated with SST and precipitation patterns similar to those observed during the recent multi-year drought period, even when the recent drought period is withheld from the calculation. Thus, the particular “flavor” of the extended La Niña episode of 1998-2002 appears to be linked to the severe drought in CSW Asia. Similarly, Kidson *et al.* (2002) used cluster analysis of OLR data to separate ENSO warm-events into two types with associated SST anomalies of differing western extent. The warm-event

type with extended Western Pacific SST anomalies is associated with stronger circulation anomalies over the Asian region.

A physical mechanism connecting Western Pacific convection and SST anomalies with CSW Asia precipitation is the wintertime upper-tropospheric westerly jet stream over subtropical east Asia and the Western Pacific, often referred to as the East Asia Jet Stream (EAJS). Yang *et al.* (2002) found EAJS strength to be inversely related with DJF CSW Asia precipitation anomalies; a strong (weak) EAJS is correlated with positive (negative) CSW Asia precipitation anomalies. Maritime Continent convection influences the EAJS through the local Hadley circulation (Chang and Lau, 1982; Chang and Lum, 1985; Lau and Boyle, 1987). Enhanced Maritime Continent convection leads to upper level divergence and southerly flow into the subtropical Northern Hemisphere. The resulting westerly flow near the EAJS exit region, due to Coriolis effect, intensifies the EAJS which in turn is associated with negative CSW Asia precipitation anomalies. The association of EAJS strengthening and upstream jet changes in the CSW Asia region seen in observations is less fully understood.

The dynamics of tropical Western Pacific heating have also been considered in modeling analyses. Sardeshmukh and Hoskins (1988) considered Rossby wave generation by tropical heating, with particular attention to Western Pacific heating. Generation of vorticity by tropical heating is often taken to be proportional to the product of mean vorticity and anomalous divergence with the mean vorticity frequently approximated for simplicity by the Coriolis parameter  $f$ . This approximation suggests only a modest response to tropical heating in the Western Pacific during Northern Hemisphere winter, both because the Coriolis force is modest near the equator and because the local flow is easterly, which should produce a critical line preventing the poleward propagation of Rossby waves. Sardeshmukh and Hoskins (1988), however, also consider the other source term for generation of vorticity: the advection of vorticity by the divergent wind.

For tropical heating in a region of easterlies, this term is actually largest near the subtropical westerly jets rather than the easterlies, and its strength is dependent on the vorticity gradient associated with the jets. By this mechanism, West Pacific Northern Hemisphere winter convection is actually a favored process for generating vorticity anomalies along the southern flank of the East Asian Jet.

Ting and Sardeshmukh (1993) showed that the steady response of a linearized dry GCM to heating is very sensitive to the basic state and heating location. In particular, the response to equatorial heating varies dramatically even within the West Pacific-Eastern Indian Ocean sector, with the largest response occurring for heating centered at 100°E (the “IPX” region of Barlow *et al.* (2002)). This sensitivity to the mean state may be a reason why GCM simulations forced by observed SSTs demonstrate little skill in simulating CSW Asia precipitation. Either GCMs are deficient in their simulation of the impact of SST anomalies on CSW Asia precipitation, or CSW Asia precipitation is not causally related to SST anomalies. Here we explore the hypothesis that SST anomalies force some portion of CSW Asia winter precipitation variability and that poor GCM simulation of CSW Asia winter precipitation is due to model deficiencies.

Statistical correction methods can compensate for model deficiencies by filling in details of large-scale teleconnection patterns found in nature but incompletely represented by models. Such methods have been used to correct model simulated precipitation anomalies (Smith and Livezey, 1999; Feddersen *et al.*, 1999) and seasonal forecasts (Mo and Straus, 2002). The fundamental idea of these methods is a multivariate (pattern) regression between model fields and observed anomalies. Principal component analysis (PCA) of model fields and observations reduces the number of degrees of freedom and decreases the effects of sampling error. Canonical correlation analysis (CCA) is used to identify model fields most highly correlated with observed precipitation anomaly patterns (Barnett and Preisendorfer, 1987). The set of CCA correspondences between model and

observation patterns is then used to predict observed precipitation anomalies from model outputs.

Here we first document the skill of the ECHAM 4.5 GCM in simulating winter precipitation in CSW Asia. We then use re-analysis wind data to elucidate connections between CSW Asia precipitation and EAJS variability, and show that the same association is not found in model simulations. We show a relation between Western Pacific precipitation and observed CSW Asia precipitation and demonstrate that this relation is present in GCM simulations forced with observed SST. This relation is sufficiently robust to be useful in hindcasts forced with imperfect, persisted SSTs.

## 2. DATA

### 2.1 *Observational data*

Seasonally averaged data from 48 December–March (DJFM) seasons 1950-51 to 1997-98 are used. Precipitation observations used to compute the skill and the statistical corrections are taken from the extended New *et al.* (2000) gridded dataset of monthly precipitation for the period of 1950 to 1998. This dataset, based on station observations interpolated to a  $0.5^\circ \times 0.5^\circ$  lat-lon grid, is here interpolated to the T42 grid of the atmospheric GCM. This dataset is used to calibrate IRI probability forecasts (Rajagopalan *et al.*, 2002). The CAMS-OPI precipitation dataset (1979-1998) which includes satellite observations is used to examine qualitative features of tropical Pacific precipitation (Janowiak and Xie, 1999). The CAMS-OPI dataset is not used to compute the skill or the statistical corrections. EAJS variability is investigated using upper level (200 hPa) wind fields from the NCEP-NCAR reanalysis (Kalnay *et al.*, 1996).

### 2.2 *Model data*

Model data is taken from two experiments: a simulation and a hindcast. The simulation data comes from a 24 member ensemble of T42 ECHAM 4.5 GCM runs forced with observed SSTs for the period 1950 to 1998 (Roeckner *et al.*, 1996). We use ensemble

means of DJFM model precipitation and upper level (200 hPa) winds. Additionally, we use data from a 30-year (1968-1998) 12-member ensemble of hindcast runs that use Dec 1 values from the above simulations as initial conditions and are forced with November observed SST anomalies added to December through March monthly climatologies.

### 3. METHODOLOGY

#### 3.1 Statistical correction

To predict the observed precipitation anomaly field  $\mathbf{x}$  from a predictor anomaly field  $\mathbf{y}$ , we assume the linear relationship  $\mathbf{x} = \mathbf{A}\mathbf{y}$  where  $\mathbf{A}$  is a suitably dimensioned regression matrix. The regression error  $\langle (\mathbf{x} - \mathbf{A}\mathbf{y})^T (\mathbf{x} - \mathbf{A}\mathbf{y}) \rangle$  is minimized by choosing  $\mathbf{A} = \langle \mathbf{x}\mathbf{y}^T \rangle \langle \mathbf{y}\mathbf{y}^T \rangle^{-1}$  where  $()^T$  denotes transpose and  $\langle \cdot \rangle$  denotes statistical expectation, here computed using time averages. There is insufficient data to determine the regression matrix  $\mathbf{A}$  when the length of the historical record is smaller than the dimensions of the anomaly fields  $\mathbf{x}$  and  $\mathbf{y}$ , and some regularization method is necessary to invert the singular predictor covariance matrix  $\langle \mathbf{y}\mathbf{y}^T \rangle$  and reduce the effect of sampling error.

A simple regularization method is to expand the observed and predictor anomaly fields in truncated Empirical Orthogonal Function (EOF) series using Principal Component Analysis (PCA). Let  $\mathbf{X}$  be the matrix whose  $i$ -th column is the observed precipitation anomaly at time  $t_i$ . Then PCA gives that  $\mathbf{X} = \mathbf{U}_x \Sigma_x \mathbf{V}_x^T$  where the columns of the orthogonal matrix  $\mathbf{U}_x$  are EOFs of the observations with normalized time-series given by the columns of  $\mathbf{V}_x$  and variances given by the squares of the elements of the diagonal matrix  $\Sigma_x$ . Likewise the predictor field can be written as  $\mathbf{Y} = \mathbf{U}_y \Sigma_y \mathbf{V}_y^T$ . Substituting these expansions into the definition of the regression matrix  $\mathbf{A}$  gives

$$\mathbf{A} = \mathbf{U}_x \Sigma_x \mathbf{V}_x^T \mathbf{V}_y \Sigma_y \mathbf{U}_y^T \mathbf{U}_y \Sigma_y^{-2} \mathbf{U}_y^T = \mathbf{U}_x \Sigma_x \mathbf{V}_x^T \mathbf{V}_y \Sigma_y^{-1} \mathbf{U}_y^T . \quad (1)$$

Difficulties caused by singularity of the predictor covariance matrix and sampling error are reduced by limiting the number of EOFs used to represent predictor and observation anomalies.

Elements of the matrix  $\mathbf{V}_x^T \mathbf{V}_y$  give the correlation of predictor and observation EOF time-series, and the singular value decomposition  $\mathbf{V}_x^T \mathbf{V}_y = \mathbf{RMS}^T$  is used in canonical correlation analysis (CCA) to identify linear combinations of observation and predictor EOFs with maximum correlation and uncorrelated time-series (Barnett and Preisendorfer, 1987). The CCA observation and predictor homogeneous covariance maps are respectively  $\mathbf{C}_x = \mathbf{U}_x \Sigma_x \mathbf{R}$  and  $\mathbf{C}_y = \mathbf{U}_y \Sigma_y \mathbf{S}$  with time-series  $\mathbf{V}_x \mathbf{R}$  and  $\mathbf{V}_y \mathbf{S}$ ; time-series correlations are given by the elements of the diagonal matrix  $\mathbf{M}$ . CCA modes with low correlation are neglected by setting the corresponding diagonal elements of  $\mathbf{M}$  to zero. Therefore determination of the regression matrix  $\mathbf{A} = \mathbf{C}_x \mathbf{M} \mathbf{C}_y^{-1}$  requires specifying the number of observation and predictor EOFs and the CCA modes (nonzero elements of the diagonal matrix  $\mathbf{M}$ ) to be used in the regression matrix  $\mathbf{A}$ . Here if a CCA mode is discarded, all CCA modes with lower correlation are also discarded. The predicted precipitation  $\mathbf{A} \mathbf{y}$  has less variance than the observed precipitation due to the error of the regression.

### 3.2 Skill evaluation

To evaluate the cross-validated skill of the CCA model, three consecutive years are selected and omitted from the calculation of the climatology, anomalies and CCA prediction model (Michaelsen, 1987). The CCA model is then used to predict the observed anomaly for the middle withheld year, and the full-field is formed by adding the climatology. Withholding each three year sequence in turn produces 48 predicted observation fields; two years are withheld for the prediction of the first and final years. We withhold three years instead of a single year in the cross-validation to ensure the

independence of the training and prediction samples, and because leaving more years out tends to select models with fewer degrees of freedom.

In addition to spatial maps of local correlations, we calculate the mean anomaly correlation, i.e., the anomaly correlation of the spatially averaged observations and simulations (Feddersen *et al.*, 1999). This measure, unlike the average correlation, reflects error in precipitation anomalies for an entire region. EOF truncations and CCA modes are chosen to maximize the cross-validated mean anomaly correlation. Maximizing the spatially averaged correlation yielded in most cases the same truncations and always yielded comparable correlation maps. Monte Carlo significance testing is used to determine correlation significance at each grid point (Livezey and Chen, 1983). Significance levels are obtained by ranking the correlations of 1000 random permutations in time of the observed data with correctly ordered observations. For the GCM simulation and other cases with 48 years of data we use the 99% significance level, and for the 30 years hindcast we use the 95% significance level. Only significant correlations are plotted.

#### 4. OBSERVED AND SIMULATED PRECIPITATION VARIABILITY

DJFM CSW Asia climatological precipitation and its variability are closely related to the elevation of the region as shown in Fig. 1. Climatological precipitation follows the principal mountain ranges of the region: the Zagros, Himalaya, Karakoram, and Hindu Kush (see Fig. 1(b)). Precipitation variability shown in Fig. 1(c) separates into two geographical regions. One accompanies the Zagros mountain range along the Southwest border of Iran. There we define the SW precipitation index as the spatial average of the precipitation in the box from 45°E to 56.25°E and from 26.5°N to 35°N (see Fig. 1(c)). Another region of substantial precipitation variability is found where the borders of Afghanistan, Pakistan and Tajikistan meet in the Hindu Kush, Karakoram and Pamir mountain ranges. We define the NE precipitation index there as the spatial average of the

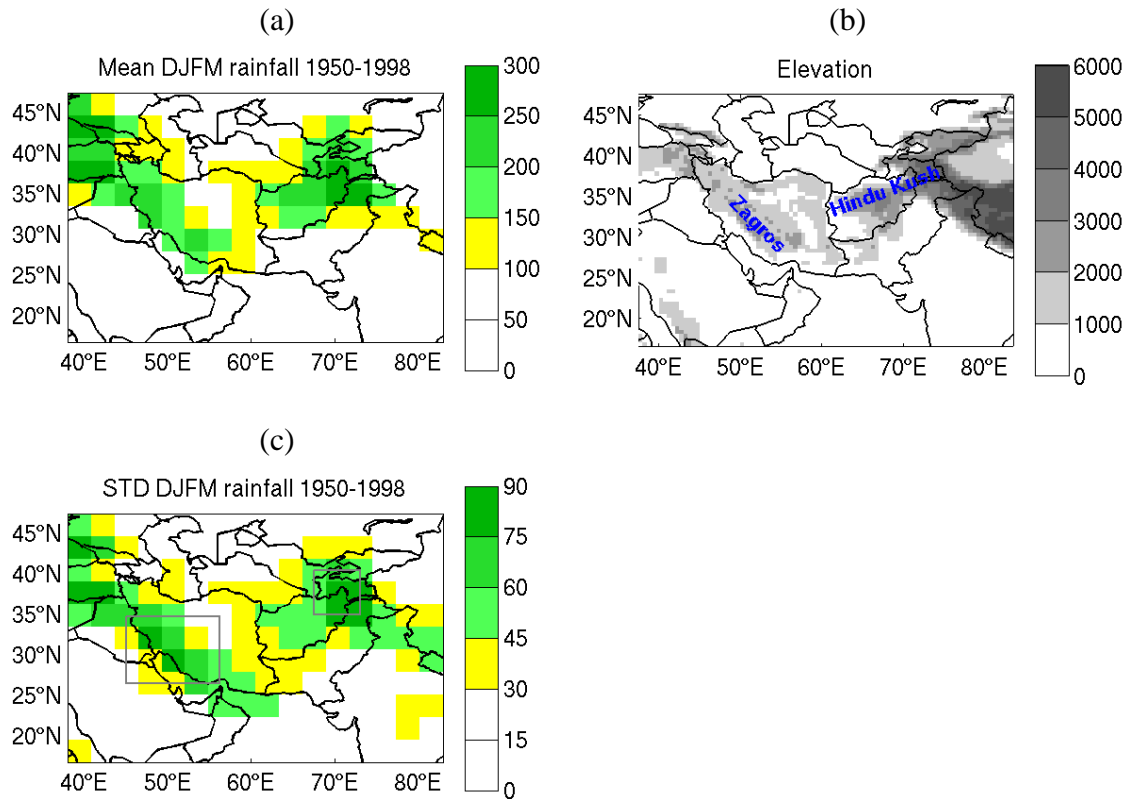


Figure 1. Panel (a) total climatological DJFM precipitation in mm, (b) elevation in meters, and (c) standard deviation of the DJFM rainfall anomalies in mm/season. The boxes in panel (c) shows the domains used to calculate NE and SW precipitation indices.

precipitation in the box from  $67.5^{\circ}\text{E}$  to  $73^{\circ}\text{E}$  and  $35^{\circ}\text{N}$  to  $45.5^{\circ}\text{N}$  (see Fig. 1(c)). The correlation between the SW and NE indices shown in Fig. 2 is 0.34, suggesting only a weak statistical relation between the precipitation variability of the two regions over the entire period, although both regions did experience drought during 1970-71 and 1998-2002. The SW and NE precipitation indices have correlations with the NINO3 index (the average SST over the region  $5^{\circ}\text{S}$  to  $5^{\circ}\text{N}$ ,  $90^{\circ}\text{W}$  to  $150^{\circ}\text{W}$ ) of 0.04 and 0.25 respectively. There is no significant statistical relation between the precipitation variability measured by these indices and ENSO activity as measured by NINO3 index. The weak 0.25 correlation between the NE and NINO3 indices hints that precipitation variability in the

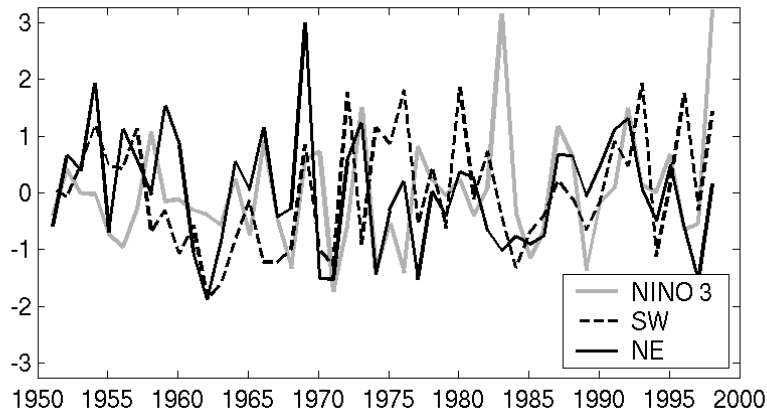


Figure 2. Standardized time-series of NE, SW and NINO3 indices.

Hindu Kush region (NE index) is more related to tropical forcing than that in the Zagros (SE index).

A typical method of determining predictable components of the climate system is to examine the simulation skill of an ensemble of atmospheric GCMs forced with observed SST. Climate components whose variability is skillfully reproduced by such simulations are driven by SST forcing and deemed predictable to the extent that SSTs can be predicted. Poor simulation skill can be due to either inherent lack of predictability or model deficiency. ECHAM 4.5 GCM simulations of DJFM CSW Asia precipitation have little skill with local correlations not exceeding 0.2 and a mean anomaly correlation of 0.1. The GCM simulations thus give no indication of predictability. In the next section we examine whether statistically transformed model outputs can be used to predict CSW Asia precipitation and correct model deficiencies.

## 5. RESULTS

We use selected ECHAM 4.5 GCM model outputs to predict CSW Asia precipitation anomalies. Observational data and previous studies identify physical mechanisms for predictability and guide our choice of predictors. EOF truncations and CCA modes are

chosen to maximize cross-validated skill. Differences between observed mechanisms and GCM simulation behavior can be attributed to absence of an SST-forced response and to model deficiencies.

### 5.1 CSW Asia regional precipitation

Using GCM simulated CSW Asia regional precipitation as a predictor gives little skill improvement relative to the uncorrected GCM output. The mean anomaly correlation of the best CCA correction model was 0.20, obtained using 3 observed precipitation EOFs, 2 simulated precipitation EOFs and 2 CCA modes. Local correlations of the corrected simulation with observations were everywhere less than 0.3. This negative result means that there is no apparent linear relation between model simulated CSW Asia precipitation and observed CSW Asia precipitation. However, this result provides no evidence to decide the question of whether poor skill is caused by a genuine lack of predictability or by model deficiencies.

### 5.2 Upper level winds

Yang *et al.* (2002) define an EAJS index as the average of the 200 hPa zonal wind in the jet maximum region  $30^{\circ}\text{N} - 35^{\circ}\text{N}$  and  $130^{\circ}\text{E} - 160^{\circ}\text{E}$ , and find negative correlations between this EAJS index and DJF precipitation anomalies in CSW Asia, as well as on the southern coast of China, South Korea and parts of Japan. Precipitation anomalies associated with EAJS variability are different from those associated with generic ENSO events, and the correlation between the EAJS index and the DJF SOI index is 0.05. Those results suggest that upper level winds are a good candidate as a predictor of CSW Asia precipitation, particularly if EAJS variability can be separated from ENSO induced wind variability.

EOF analysis of the DJF 200 hPa zonal wind by Yang *et al.* (2002) in the domain  $0^{\circ}$  to  $60^{\circ}\text{N}$  and  $60^{\circ}\text{E}$  to  $120^{\circ}\text{W}$  indicates that the leading EOF is related to ENSO variability and has most of its structure east of the date line. The second EOF has

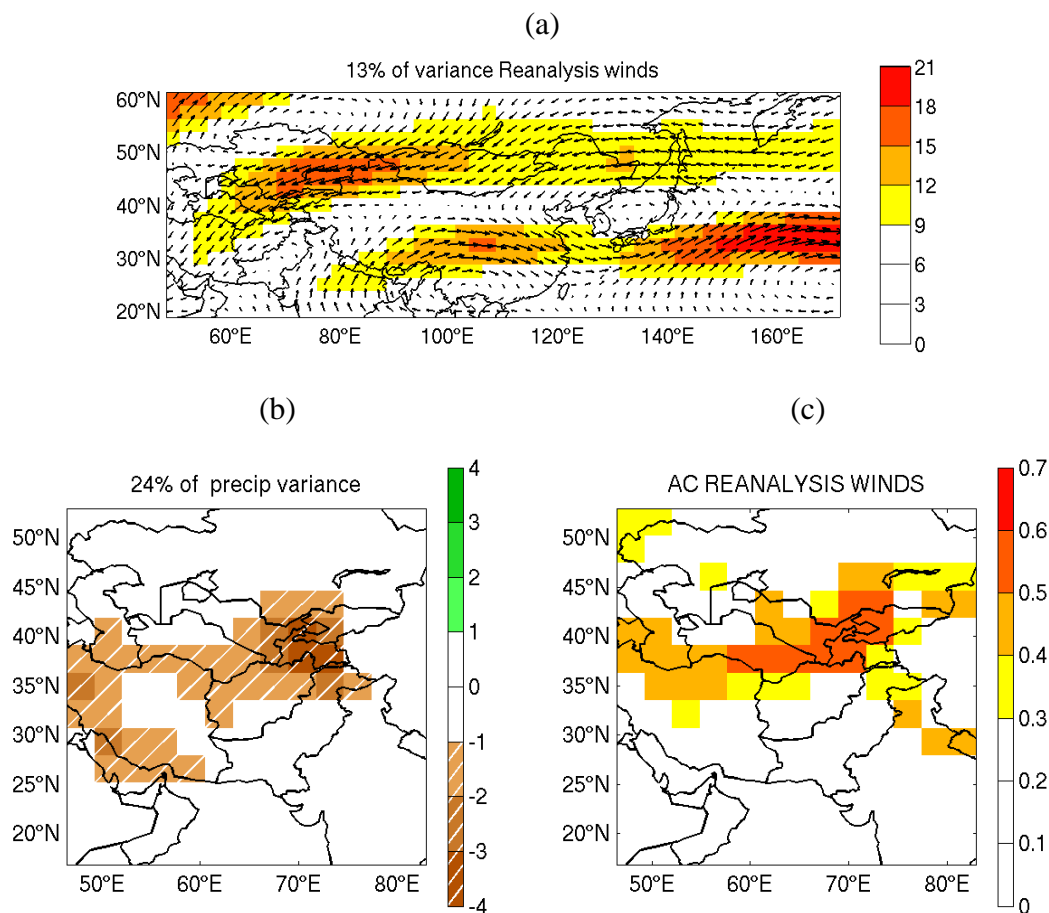


Figure 3. Homogeneous covariance maps for (a) 200 hPa observed winds (m/s) (shading indicates wind speed) and (b) observed precipitation (mm/day). (c) Anomaly correlation using observed wind anomalies to predict simultaneous precipitation.

strong zonal structure over Asia, in particular over the jet maximum region and Western Pacific. Therefore, we focus our analysis on EAJS variability and consider the NCEP-NCAR reanalysis 200 hPa wind field anomaly in the domain 50°E to 170°E and 20°N to 60°N, excluding the region where the ENSO impact on upper level winds is largest. The EOF analysis of Yang *et al.* (2002) shows that strengthening of EAJS index corresponds to westward and southward shifts of the jet structure east of about 75°E. We consider wind field anomalies rather than only zonal wind anomalies to capture meridional flow anomalies associated with these shifts of the EAJS.

The first EOF of the 200 hPa wind field (not shown) explains 22% of the observed variance, and the correlation of its time-series with the NE precipitation index is 0.50; the correlation of the first wind EOF time-series with the SW and NINO3 indices is 0.36 and -0.14, respectively. The first EOF of the 200 hPa wind field shows southwesterly flow over CSW Asia and is positively correlated with positive CSW Asia precipitation anomalies, consistent with an interpretation of enhanced southwesterly winds over elevation leading to enhanced upwind precipitation. A correction model using only the first wind anomaly and precipitation EOFs results in a cross-validated mean anomaly correlation of 0.48.

The leading homogeneous covariance fields of a CCA model using 7 observed precipitation EOFs, 10 observed wind EOFs and 2 CCA mode are shown in Figs. 3(a) and 3(b). The cross-validated mean anomaly correlation of this CCA correction model is 0.65 and the correlation map is shown in Fig. 3(c). Figure 3(a) shows that the homogeneous covariance wind anomaly field over Afghanistan is northeasterly with structure similar to the first wind field EOF. Figure 4 shows the time-series (not cross-validated) of the leading CCA modes; the time-series multiply the homogeneous covariance patterns in Fig. 3(a) and (b). The five year period of the reanalysis wind time-series after 1998 is independent of the CCA analysis and indicates that during the 1998-2002 drought period there were wind anomalies associated with negative precipitation anomalies and that during the flooding of 2003<sup>‡</sup> there were wind anomalies associated with positive precipitation anomalies.

Since observed upper level winds are a reasonably good predictor of CSW Asia precipitation, we now take ECHAM 4.5 model simulated winds as predictors. However, the skill of the best correction model (8 observation EOFs, 9 model wind EOFs and 3 CCA modes) is poor with cross-validated mean anomaly correlation of 0.27 and

<sup>‡</sup> See <http://www.irinnews.org/report.asp?ReportID=34403> a report from the Integrated Regional Information Networks (IRIN), a part of the UN Office for the Coordination of Humanitarian Affairs (OCHA).

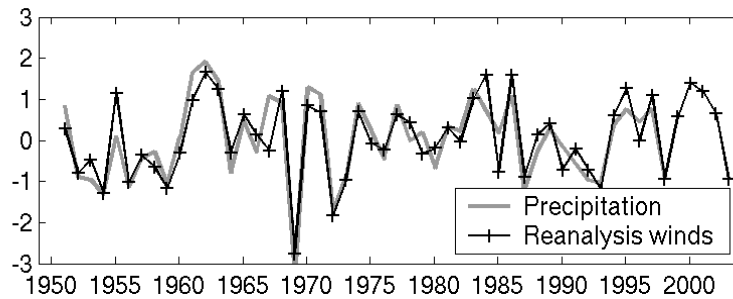


Figure 4. Standardized time-series of wind and precipitation CCA modes winter 1950-51 through winter 2002-03. Wind time-series after 1998 is independent.

correlations exceeding 0.3 at only a single grid point. Model simulated winds may be a poor predictor because the GCM responds incompletely to SST forcing or because the observed wind variability related to CSW Asia precipitation is driven by internal variability rather than SST forcing. The precipitation homogeneous covariance pattern (not shown) is similar to that obtained using observed winds (Fig. 3b). However, the model wind homogeneous covariance pattern is strikingly different from the observed wind pattern in Fig. 3a and resembles the pattern obtained by regressing the NINO3 index onto the observed wind field. In fact, the correlation between the model wind pattern and NINO3 is -0.61. In contrast, the correlation between NINO3 and reanalysis wind CCA modes 1 and 2 is -0.22 and 0.26 respectively. Additionally, the first EOF of the model winds is well correlated with ENSO while the first EOF of the observed winds is not; similar conclusions are true for individual ensemble members. Simulated upper-level wind variability is more related to ENSO than is observed upper-level wind variability.

### 5.3 Western tropical precipitation

EAJS variability is associated with convection in the Western Pacific and Maritime Continent (Chang and Lau, 1982; Chang and Lum, 1985; Lau and Boyle, 1987; Yang *et al.*, 2002). Maritime Continent convection and the EAJS are coupled through the local East Asia Hadley circulation with correlation between the Maritime Continent and EAJS

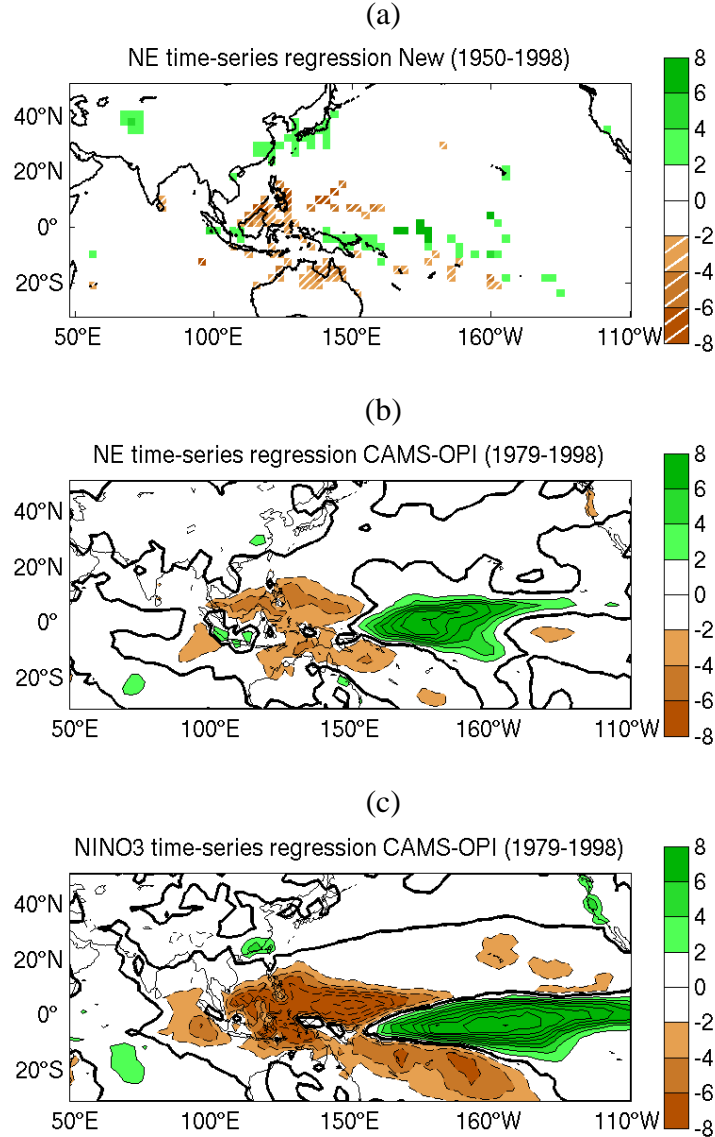


Figure 5. Regression of the NE time-series onto (a) DJFM New *et al.* (2000) precipitation data 1950-1998 and (b) CAMS-OPI precipitation data (1979-998). (c) Regression of Niño 3 index onto CAMS-OPI precipitation data. Negative contours are dashed. Contour interval is 2 mm/day; zero line is heavy. Units are mm/day.

being the result of the Coriolis effect acting on the North-South divergent outflow from the Maritime Continent (Lau and Boyle, 1987). Enhanced Maritime Continent convection and anomalous ascending motion are associated with upper-level divergent flow away from the equator. In the Northern Hemisphere this southerly flow leads to an upper-level

westerly anomaly. This westerly anomaly strengthens the EAJS which is accompanied by negative precipitation anomalies over CSW Asia. The causality of the relation between Maritime Continent convection and EAJS strength is less clear. However, Chang and Lum (1985) examining lead-lag relationships between tropical divergence and acceleration of the subtropical jet, show tropical forcing preceding jet acceleration, and specifically note that convective activity in the Indian Ocean could result in a significant longitudinal displacement of the EAJS.

Lau and Boyle (1987) emphasize that Maritime Continent and Central Pacific convective forcing produce very different extratropical responses, particularly in the wind fields, with the overall streamfunction response in the extratropics being more sensitive to Maritime Continent forcing than to forcing in the Central Pacific. Kidson *et al.* (2002) also find that the response to tropical forcing differs according to whether the forcing is in the Central Pacific or in the Maritime Continent. Using cluster analysis of OLR data, they separate warm tropical SST events into two types, one of which (“EN”) has influence in the EAJS region. The Hadley Centre GCM used in that study was not able to distinguish between the two forcings although simpler models did.

Barlow *et al.* (2002) considered the ENSO signal stratified into two patterns based on the strength of the SST anomalies in the West Pacific. This stratification resulted in different tropical precipitation anomaly patterns in the West Pacific-Eastern Indian Ocean and associated differences in atmospheric and precipitation anomalies extending into Asia. The ENSO stratification with the more vigorous West Pacific SST signal was associated with a pattern very similar to the recent drought in both SSTs and precipitation.

The regression of the NE time-series on to New *et al.* (2000) precipitation data is shown in Fig. 5a. The NE time-series is associated with positive precipitation anomalies in western China, Korea and Southern Japan as well as east-west gradient in the Maritime Continent region. The Maritime Continent precipitation pattern is clearer in Fig. 5b where

satellite-based CAMS-OPI data is used. § The precipitation pattern associated with the NE time-series is different from the classical ENSO pattern shown in Fig. 5c. The NE pattern has a weak negative anomaly to the west of a strong positive anomaly while the ENSO pattern has more balanced positive and negative anomalies. The tropical anomalies in the NE patterns are primarily to the west of 160W while the ENSO patterns extends further to the east. The NE pattern resembles the OLR pattern (“EN”) that Kidson *et al.* (2002) associated with ENSO episodes having enhanced western extension of SST anomalies.

GCM simulated precipitation in the Western Pacific and Maritime Continent is to a large extent driven by prescribed local SSTs and is relatively realistic. Therefore, GCM simulated precipitation in the Western Pacific and Maritime Continent was used to estimate CSW Asia precipitation. Using 8 observation EOFs, 7 simulation EOFs and 4 CCA modes gives a mean anomaly correlation of 0.47. The mean anomaly correlation is relatively low but regionally some areas in the NE region have corrections above 0.4. For this reason, we chose a smaller area around the NE region and performed the statistical corrections using this domain (see Fig. 6(b)). The best correction model uses 2 observation EOFs, 2 model precipitation EOFs and 2 CCA modes. The leading homogeneous covariance fields are shown in Figs. 6(a) and 6(b). The cross-validated mean anomaly correlation is 0.54 and the correlation map is shown in Fig. 6(c); root-mean-square (RMS) errors are shown for the uncorrected simulation and the corrected prediction in Figs. 6(d) and 6(e).

Although Western Pacific GCM simulated precipitation is highly correlated with observed SSTs, we find that GCM simulated precipitation is a modestly better predictor than SST; the cross-validated mean anomaly correlation is 0.46. This difference may be

§ The lack of signal in the NE region of Fig. 5b is due to the different periods used and data issues in the region: the variance of the NE time-series during the common period 1979-1998 is 40.3 mm/season when computed with the New *et al.* (2000) data and 29.5 mm/season when computed with the CAMS-OPI data; the correlation of the two NE time-series is 0.81.

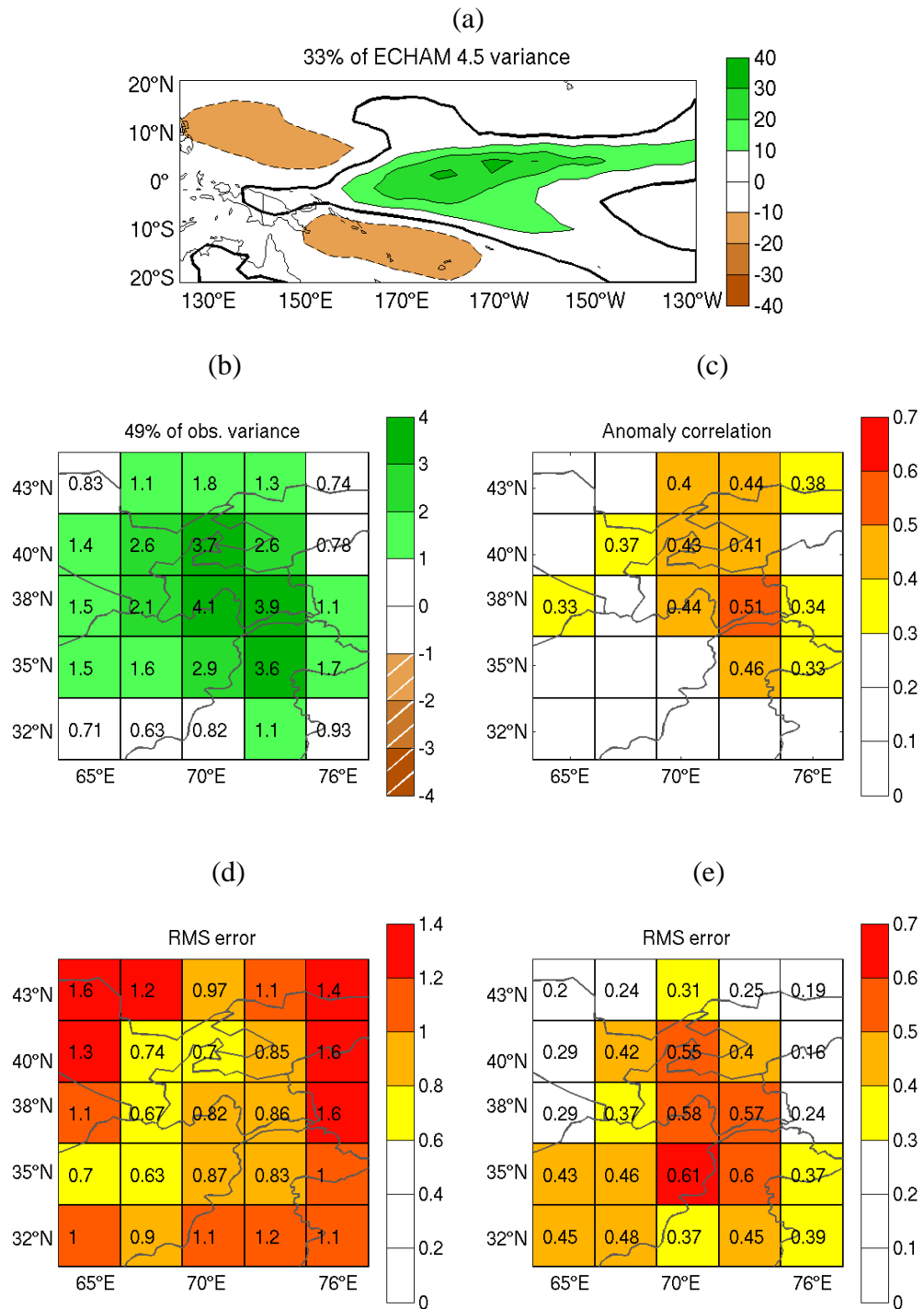


Figure 6. Homogeneous covariance maps for (a) ECHAM 4.5 Western Pacific simulated precipitation (negative contours are dashed; contour interval is 10 mm/day; zero line is heavy) (b) observed CSW Asia precipitation (mm/day). (c) Anomaly correlation of the CCA model. RMS error of the (d) raw GCM simulation and (e) corrected predictions in mm/day.

chance or may be related to the fact that precipitation is a nonlinear function of SST and is more directly related to heating that drives circulation anomalies.

While simulation results represent the upper limit of skill when the SST is perfectly known, in practice one cannot predict SST perfectly. To obtain a more realistic estimate of forecast skill, we apply the same method to hindcasts that use persisted SST anomalies instead of observed ones. Three observation EOFs, 4 model EOFs and 2 CCA modes were used to construct the correction model. The leading homogeneous covariance fields are shown in Figs. 7(a) and 7(b). The cross-validated mean anomaly correlation is 0.36 and the correlation map is shown in Fig. 7(c). RMS errors are shown for the uncorrected hindcast and the corrected prediction in Figs. 7(d) and (e). Although skill is lost compared to that using observed SST, some correlations are above 0.4, a correlation level usable in seasonal prediction (personal communication, A. Barnston).

## 6. SUMMARY AND CONCLUSIONS

Drought and its severe societal impacts makes seasonal forecasts of Central South-west (CSW) Asia precipitation highly desirable. Observational studies show links between CSW Asia precipitation, East Asia Jet Stream (EAJS) variability and Maritime Continent convection. However, atmospheric GCMs forced by observed SSTs do not reproduce these relations. In particular the ECHAM 4.5 model does not simulate well CSW Asia winter precipitation. Other GCMs from NCEP, COLA and NSIPP used in IRI seasonal forecasts present comparable simulation skill (personal communication, A. Barnston). Poor simulation skill can be due to either lack of a response to SST forcing or failure of the model to reproduce that response correctly.

Here we have examined statistical methods of correcting systematic errors in GCM simulations of CSW Asia precipitation using canonical correlation analysis. The statistical corrections generally had most success in the region where the borders of Afghanistan, Pakistan and Tajikistan meet and no success in the region along the Southwest border of

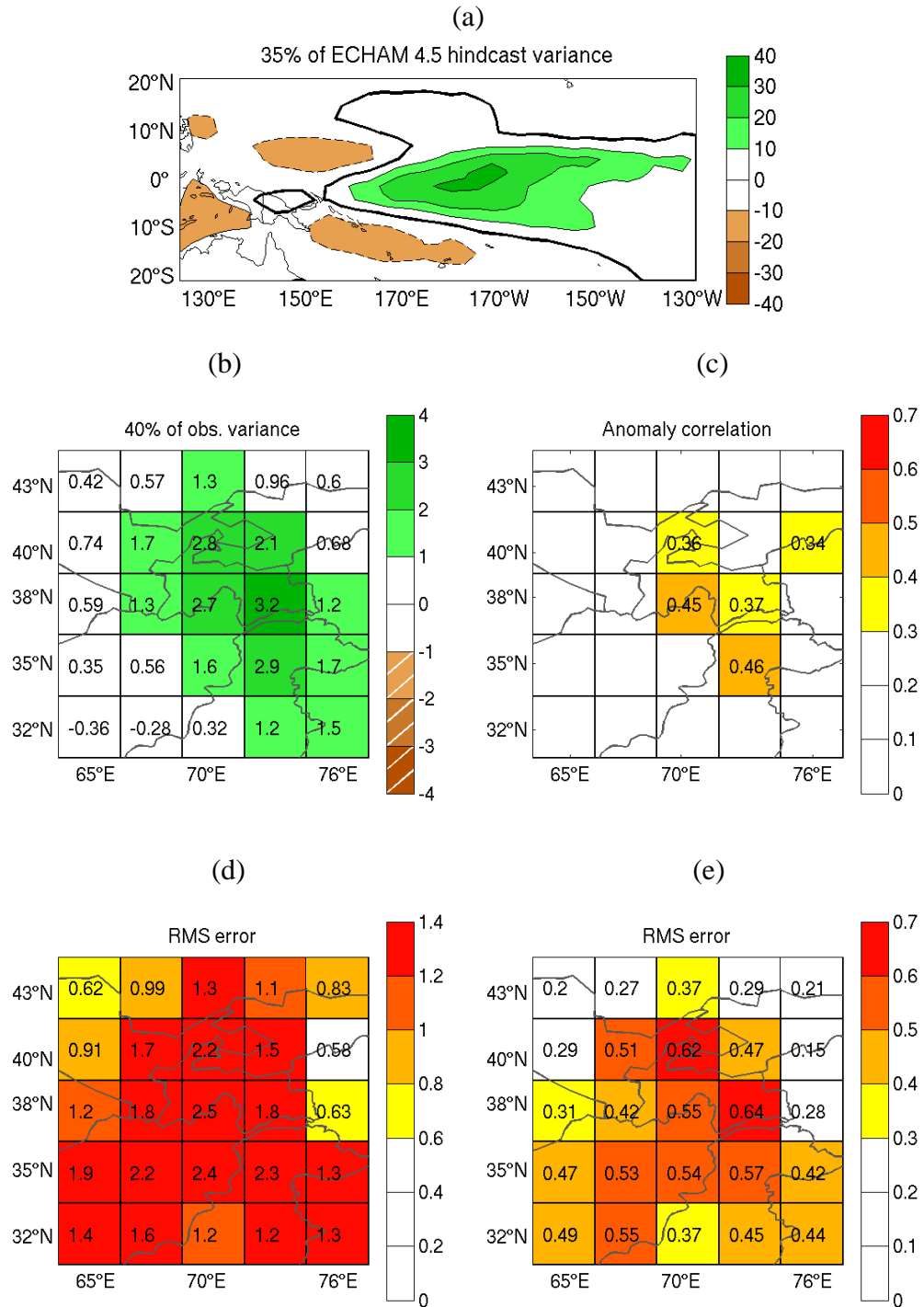


Figure 7. Homogeneous covariance maps for (a) ECHAM 4.5 Western Pacific hindcast precipitation (negative contours are dashed; contour interval is 10 mm/day; zero line is heavy) (b) observed CSW Asia precipitation (mm/day). (c) Anomaly correlation of the CCA model. RMS error of the (d) raw GCM hindcast and (e) corrected predictions in mm/day.

Iran. We found that ECHAM 4.5 GCM regional precipitation was a poor predictor of observed precipitation anomalies. However, observed CSW Asia precipitation anomalies are related to EAJS variability and we found that *observed* upper-level winds were a good predictor of observed precipitation anomalies. *Simulated* model winds were a poorer predictor.

EAJS variability is also related to Maritime Continent convective forcing. For this reason, Western Pacific model precipitation, which is simulated relatively realistically, has some modest skill as a predictor of CSW Asia precipitation anomalies. This relation appears robust, and is seen not only in ECHAM 4.5 model simulations but also in in hindcasts using persisted SST anomalies and in other GCMs simulations.

#### ACKNOWLEDGMENTS

Two anonymous reviewers provided useful comments and suggestions. We thank Matayo Indeje for his useful comments on this manuscript, and Tony Barnston for his encouragement, suggestions and numerous discussions, particularly on the application of CCA methods. We thank Benno Blumenthal for the IRI Data Library. IRI is supported by its sponsors and NOAA Office of Global Programs Grant number NA07GP0213.

#### REFERENCES

- Agrawala S, Barlow M, Cullen H, Lyon B. 2001. The Drought and Humanitarian Crisis in Central and Southwest Asia: A Climate Perspective. IRI Report. IRI, Palisades, NY, 24 pp. Available online at:  
<http://iri.columbia.edu/outreach/publication/irireport/SWAsia/index.html>.
- Barlow M, Cullen H, Lyon B. 2002. Drought in Central and Southwest Asia: La Niña, the Warm Pool, and Indian Ocean Precipitation. *Journal of Climate*. **15**: 697–700.

- Barnett TP, Preisendorfer R. 1987. Origins and Levels of Monthly and Seasonal Forecast Skill for United States Surface Air Temperatures Determined by Canonical Correlation Analysis. *Monthly Weather Review*. **115**: 1825–1850.
- Chang, C.-P. and K. Lau, 1982. Short-Term Planetary-Scale Interactions over the Tropics and Midlatitudes during Northern Winter. Part I: Contrasts between Active and Inactive Periods. *Monthly Weather Review*. **110**: 933–946.
- Chang C-P, Lum K. 1985. Tropical-Midlatitude Interactions over Asia and the Western Pacific Ocean during the 1983/84 Northern Winter. *Monthly Weather Review*. **113**: 1345–1358.
- Feddersen H, Navarra A, Ward MN, 1999. Reduction of Model Systematic Error by Statistical Correction for Dynamical Seasonal Predictions. *Journal of Climate*. **12**: 1974–1989.
- Janowiak J, Xie P. 1999. CAMS-OPI: A Global Satellite-Rain Gauge Merged Product for Real-Time Precipitation Monitoring Applications. *Journal of Climate*. **12**: 3335–3342.
- Kalnay E and Coauthors. 1996. The NCEP/NCAR 40-Year Re-analysis Project. *Bulletin of the American Meteorological Society*. **77**: 437–471.
- Kidson JW, Revell MJ, Bhaskaran B, Mullan AB, Renwick JA. 2002. Convection Patterns in the Tropical Pacific and Their Influence on the Atmospheric Circulation at Higher Latitudes. *Journal of Climate*. **15**: 137–159.
- Lau KM, Boyle JS. 1987. Tropical and Extratropical Forcing of the Large-Scale Circulation: A Diagnostic Study. *Monthly Weather Review*. **115**: 400–428.
- Livezey RE, Chen W. 1983. Statistical Field Significance and its Determination by Monte Carlo Techniques. *Monthly Weather Review*. **111**: 46–59.

- Martyn D. 1992. *Climates of the world*. Elsevier. 436 pp.
- Michaelsen J, 1987. Cross-Validation in Statistical Climate Forecast Models. *Journal of Climate and Applied Meteorology*. **26**: 1589–1600.
- Mo R, Straus DM, 2002. Statistical-Dynamical Seasonal Prediction Based on Principal Component Regression of GCM Ensemble Integrations. *Monthly Weather Review*. **130**: 2167–2187.
- Nazemosadat M, Cordery I, 2000. On the relationships between ENSO and autumn rainfall in Iran. *International Journal of Climatology*. **20**: 47–61.
- New MG, Hulme M, Jones PD. 2000. Representing 20th century space-time climate variability. II: Development of 1901-1996 monthly terrestrial climate fields. *Journal of Climate*. **13**: 2217–2238.
- Rajagopalan B, Lall U, Zebiak SE. 2002. Categorical Climate Forecasts through Regularization and Optimal Combination of Multiple GCM Ensembles. *Monthly Weather Review*. **130**: 1792–1811.
- Roeckner E, Arpe K, Bengtsson L, Christoph M, Claussen M, Dümenil L, Esch M, Giorgetta M, Schlese U, Schulzweida U. 1996. The atmospheric general circulation model ECHAM-4: Model description and simulation of present-day climate. Technical Report 218, Max-Planck Institute for Meteorology, Hamburg, Germany, 90 pp.
- Ropelewski C, Halpert M. 1987. Global and Regional Scale Precipitation Patterns Associated with the El Niño/Southern Oscillation. *Monthly Weather Review*. **115**: 1606–1626.
- Ropelewski C, Halpert M. 1989. Precipitation Patterns Associated with the High Index Phase of the Southern Oscillation. *Journal of Climate*. **2**: 268–284.

- Sardeshmukh P, Hoskins B. 1988. The Generation of Global Rotational Flow by Steady Idealized Tropical Divergence. *Journal of Atmospheric Sciences*. **45**: 1228–1251.
- Smith TM, Livezey RE. 1999. GCM Systematic Error Correction and Specification of the Seasonal Mean Pacific-North America Region Atmosphere from Global SSTs. *Journal of Climate*. **12**: 273–288.
- Ting M, Sardeshmukh P, 1993. Factors Determining the Extratropical Response to Equatorial Diabatic Heating Anomalies. *Journal of Atmospheric Sciences*. **50**: 907–918.
- Yang S, Lau K-M, Kim K-M. 2002. Variations of the East Asian Jet Stream and Asian-Pacific-American Winter Climate Anomalies. *Journal of Climate*. **15**: 306–325.